Int. J. Electrochem. Sci., 14 **(2019)** 10198 – 10212, doi: 10.20964/2019.11.26

International Journal of
ELECTROCHEMICAL
SCIENCE
www.electrochemsci.org

Porous Carbon Electrode Derived from Waste Wine Industry for Supercapacitors

Diancheng Duan[1#], WeiSu[1#], Xiyou Tan[2], Fang Hu[1], Yangyang, Wang[1], Weiyou Huang[1], Hongliang Peng[1,], Fen Xu[1], Yongjin Zou[1], Lixian Sun[1,*]*

[1] Guangxi Key Laboratory of Information Material, Guangxi Collaborative Innovation Center of Structure and Property for New Energy and Materials, School of Material Science and Engineering, Guilin University of Electronic Technology, Guilin, 541004, P. R. China
[2] Supervisory Office of the Joint Logistics Department of Guangzhou Military Region
[#]They contributed equally to this work
[*]E-mail: hlpeng2005@126.com (Hongliang Peng), sunlx@guet.edu.cn(Lixian Sun)

Received: 4 July 2019 / *Accepted:* 28 August 2019 / *Published:* 7 October 2019

Using porous carbon derived from waste biomass as electrode material for supercapacitors is a hot topic. It reuses waste at low cost. In this work, JZn-850 is prepared from waste wine industry by treatment with $ZnCl_2$. JZn-850 BET surface area is up to 1103 m^2 g^{-1}. And it exhibits specific capacitance is 187 F g^{-1} at the current density of 0.5 A g^{-1}. This is better than other commercial carbon materials such as carbon nanotubes (36 F) and graphene oxide (162 F). JZn-850 also has superior rate capability, from 0.5A g^{-1} to 20 A g^{-1}; its specific volume retention rate is 83.8%. As a new type of electrode material, it has potential applications in supercapacitors and other energy storage materials.

Keywords: Supercapacitors; Carbon materials; Biomass; Waste wine industry.

1. INTRODUCTION

Over the past few decades, green and efficient energy storage and conversion technologies are developing rapidly [1-14]. Supercapacitors have received a lot of attention for their fast charging and discharging speed, large power, high stability [15-18]. Double-layer supercapacitors (DLCs), in particular, have efficient and stable energy storage and transmission because they do not involve chemical reactions [19-23]. In recent years, scholars have made great progress in the research of DLCs [24-26]. However, high cost activated carbon materials with ultra-high surface area are often used as electrode materials in commercial applications [27-30], in order to obtain excellent energy and power densities. A key challenge is to develop cheap and efficient carbon materials with excellent energy storage properties.

Biomass is an ideal raw material for carbon materials because of its wide source, low price and abundant heteroatom. In fact, biomass has been widely used in electrochemical catalysis and energy storage [31-33]; they can be directly carbonized to prepare high quality activated carbon materials. Song et al.[32] have direct pyrolysis the Corn husk which has by KOH pre-treatment, and obtain an activated carbon material with high specific capacitance of 356 F g^{-1}. Biomass often contains a variety of heteroatom, which can change the molecular orbital and charge distribution on the surface of carbon materials[34]. Xu et al. [31] have carbonized broad bean and obtain a sulfur and nitrogen co-doped activated carbon material which has specific capacitance (202 F g^{-1}) and superior cycling performance. In recent years, in order to protect the natural ecology, scholars tend to use waste biomass materials [35-37]. However, the energy density of supercapacitors is far less than that of lithium-ion batteries, Zn-air batteries or fuel cell [38-44]. It is of great significance to explore some new biomass carbon materials and apply them to supercapacitors.

In this work, we present a simple method for a new biomass carbon materials derived from waste wine industry. Generally speaking, Wine Co. will produce a large amount of wasting wine industry every day. If this waste is not dealt with in time, it will cause environmental pollution and the waste of resources. Interestingly, we prepare the carbon materials which derived from waste wine industry have excellent energy storage properties, and it has potential applications in the electrode materials of supercapacitor.

2. EXPERIMENTAL

2.1. Preparation

We prepared waste wine industry derived carbon materials as following: firstly, waste wine industry was washed with deionized water, then dried at 85 ^{o}C for 72 h and ground into a fine powder. Secondly, 3 g of this wine residue powder was activated by $ZnCl_2$ solution for 24 h (the amount of zinc chloride is ca. 30 wt %), followed by vacuum drying at 85 ^{o}C. Then the powder was heated at a rate of 5 ^{o}C min^{-1} in N_2 flow (20 sccm). The classic carbonization procedure is described in our previous manuscript[33]: (1) at 200 ^{o}C for 1 h to remove the adsorbed water; (2) at 400 ^{o}C for 1 h to dehydrate and carbonize the material; (3) at 800 ◦C (or 850 ◦C, 900 ◦C and 900 ◦C) for 2 h to further carbonize and graphitize the material. Finally, the sample was leached with 3 M HCl solution at 80 ^{o}C for 2 h, followed by heat treatment at 800 ^{o}C (or 850 ^{o}C, 900 ^{o}C and 900 ^{o}C) for 1 h. We designate the carbon materials as JZn-800, JZn-850, JZn-900 and JZn-950.

For comparison, we prepared J-850 sample by directly pyrolyzing waste wine industry without $ZnCl_2$ activation. The other procedures are similar to those used to prepare the JZn-850.

2.2. Physical characterisation

Raman characterization was carried out with a laser confocal Raman spectroscopy (Lab RAM HR Evolution, Horiba JY, France) employing a 532 nm laser beam. Scanning electron microscopy

(SEM, JSM-6360LV, JEOL Ltd., Japan) and transmission electron microscopy (TEM, Talos F200X, FEI Ltd., USA) were used to characterize the morphology and microstructure. Nitrogen sorption isotherms were measured on a gas adsorption analyzer (Autosorb iQ2, Quanta chromesor ptometer, USA) at 77K. Before measurement, the samples were degassed at 80 °C for 2 h and then 150 °C for 10 h. The specific surface area (SSA) was acquired using BET equation, and the pore size distribution (PSD) was determined based on the adsorption branches of the isotherms. The X-ray diffractometer(XRD) uses Buker-D8 Advance made in Germany and uses Cu Kα light source with a step of 0.01°, The surface functionalities and chemical composition were characterized by X-ray photoelectron spectrometer (XPS, Escalab250Xi, Thermo Fisher, USA) with an Al Kα excitation source.

2.3. Electrochemical measurements

The electrochemical measurement system is a three-electrode system for measuring the working electrode / HgO reference electrode / Pt sheet electrode. The electrode is an active material, acetylene black and polytetrafluoroethylene (8: 1: 1, mass ratio), evenly mixed, and pressed on a nickel foam collector. The electrolyte uses a 6.0 M KOH solutions, using galvanostatic charge-discharge (GCD), cyclic voltammetry (CV) and electrochemical impedance spectroscopy (EIS). EIS was performed in a frequency range from 100 kHz to100 mHz with an amplitude of 5 mV on a Zahner IM6e electrochemical workstation. GCD and CV tests were conducted on a CHI660e electrochemical workstation (Chenhua Instrument Inc.). All the electrochemical tests were carried out.

3. RESULTS AND DISCUSSION

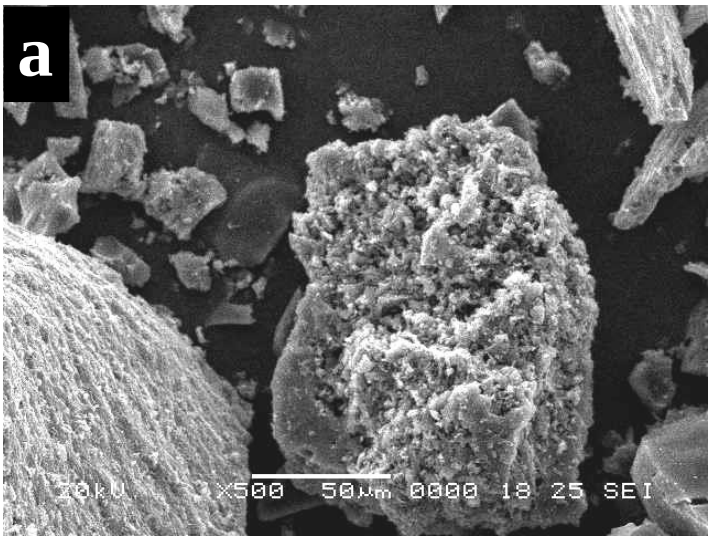

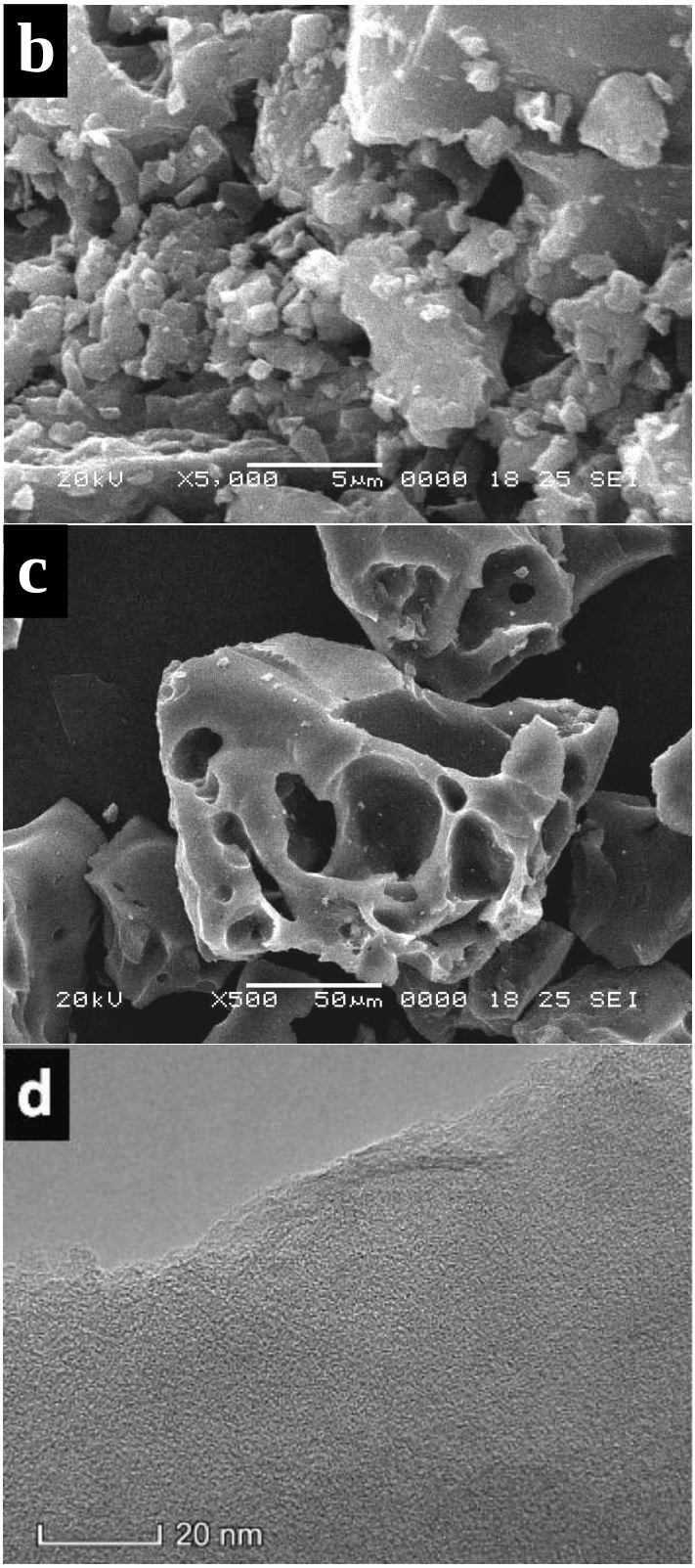

Figure 1. SEM images J-850 (a, b), JZn-850 (c); and TEM image of J-850 (d).

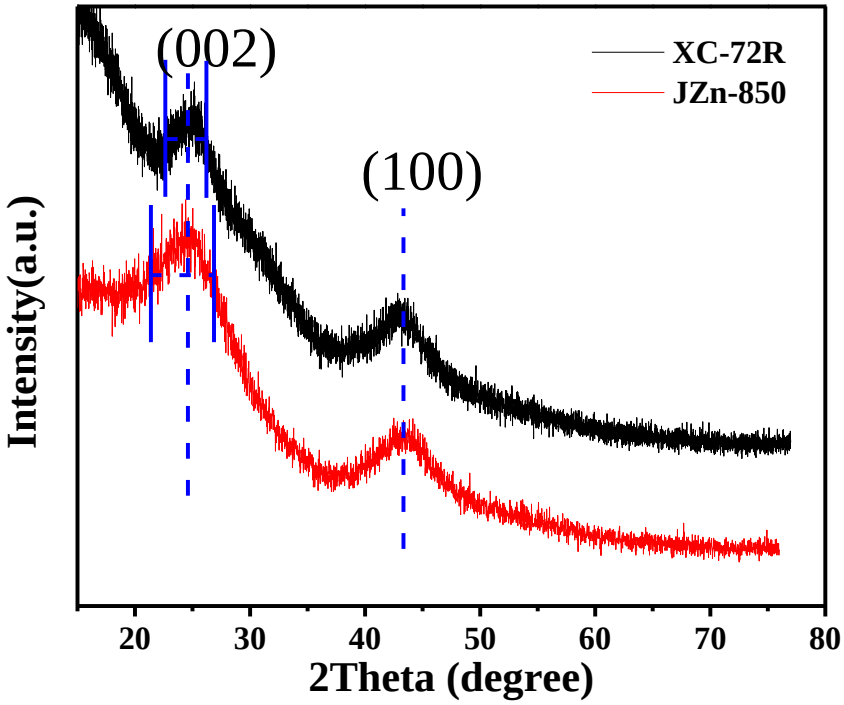

Figure 2. XRD patterns of JZn-850 and Vulcan XC-72R.

The SEM and TEM images of J-850 and JZn-850 are shown in Fig. 1. Fig.1a shows that the carbon material J-850 has a blocky structure. With a further magnification of the J-850, as shown in Fig. 1b, the carbon material is bright and clean, there is no pore structure is found. However, Fig. 1c shows that JZn-850 has a porous structure and different pore sizes, which are mainly due to the activation of $ZnCl_2$. We believe that there must be many micropores in the carbon material JZn-850. However, we cannot observe more micropores in JZn-850 material from Fig. 1d. The pore size of these micropores is too small to be observed by TEM. We can be observed from Fig. 1d that the carbon material JZn-850 is mainly amorphous carbon structure.

XRD patterns of JZn-850 and Vulcan XC-72R carbon material are shown in Fig. 2. We observed that JZn-850 and Vulcan XC-72R have similar XRD patterns; this suggests that they all have similar carbon material structures. In addition, we also found that the Full-Width Half-Maximum (FWHM) 002 peak of JZn-850 is about 1.5 times that of Vulcan XC-72R. This indicates that the crystallinity of JZn-850 is lower than that of Vulcan XC-72R. This is explained by the fact that the carbon material becomes porous after being activated by $ZnCl_2$, and reducing its degree of graphitization. This conclusion is consistent with SEM and TEM conclusions.

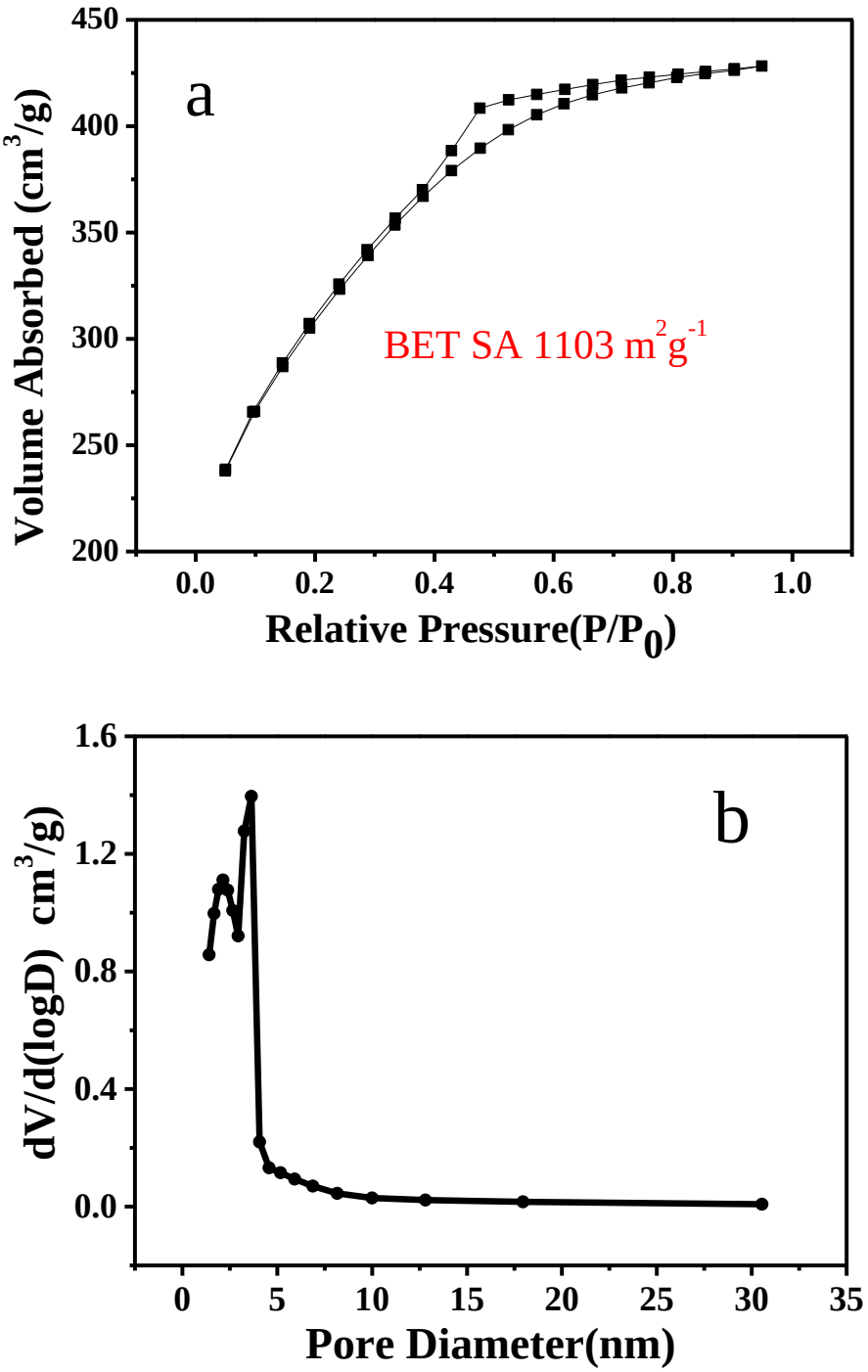

Figure 3. (a) N_2 adsorption–desorption isotherms, and (b) corresponding pore-size distribution of JZn-850

We have found that JZn-850 has a large number of macropores, which is formed by the activated of $ZnCl_2$. From this, we can infer that there must be many micropores and mesopores, in the material JZn-850. In order to confirm our hypothesis, we have performed nitrogen sorption isotherms characterization of JZn-850.

Fig. 3a shows the N_2 adsorption–desorption isotherms and BJH pore size distribution of JZn-850. The JZn-850 yield a type-I curve with an H2 hysteresis loop[45, 46]. And the BET surface area of JZn-850 is 1103 m^2g^{-1}. As shown in Fig 3a, we find that in the low relative pressure region, the gas adsorption has a rapid growth. This is due to microporous filling [47, 48]. And the H2 hysteresis loop is due to some irregular mesopores and macropores. As Fig. 3a shown, the pore size distributed ranges of the JZn-850 is mainly from between 1.4 nm to 10 nm, and there are two peaks at the pore diameter of 2.1 nm and 3.6 nm. This proves to be large number of micropores and mesopores in JZn-850.

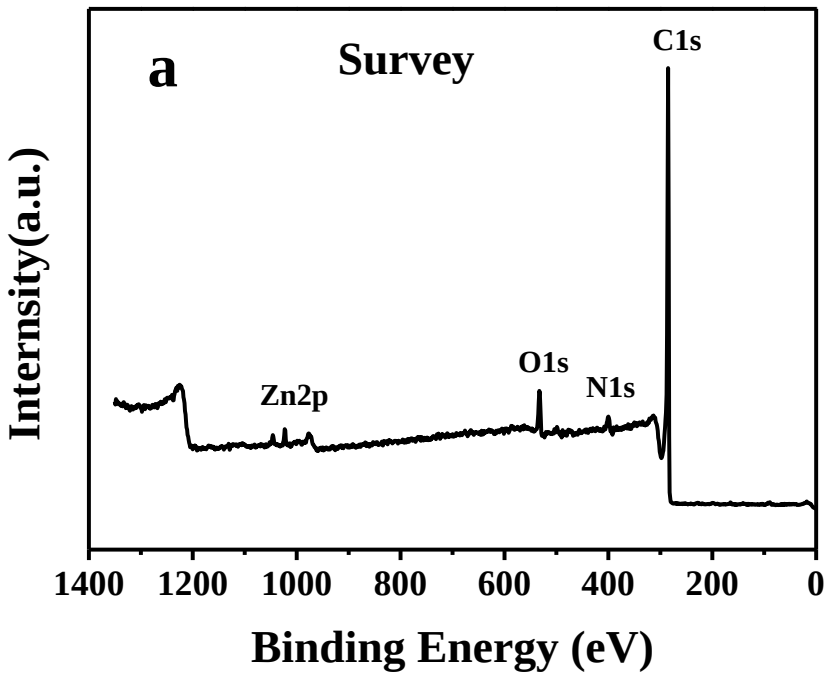

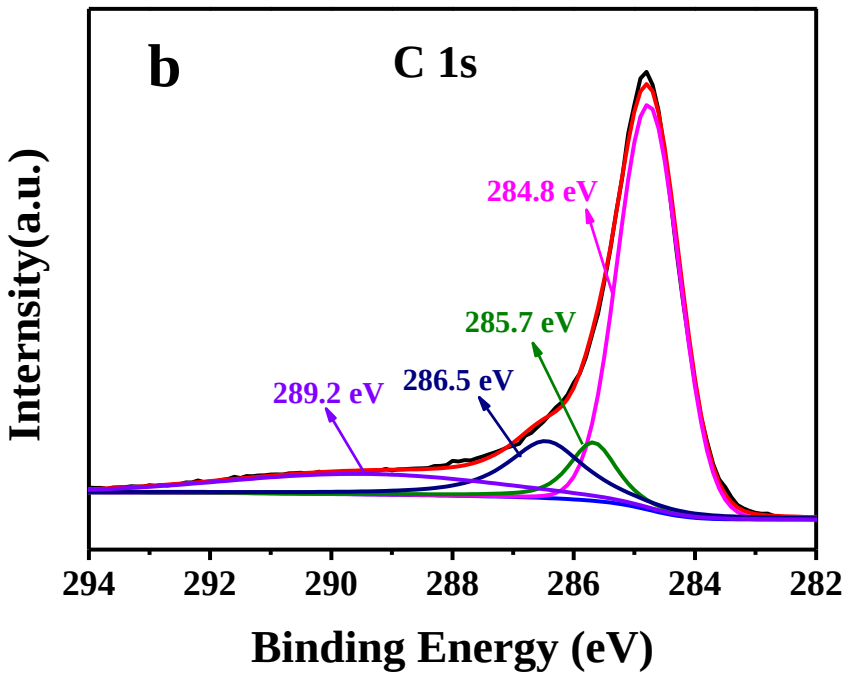

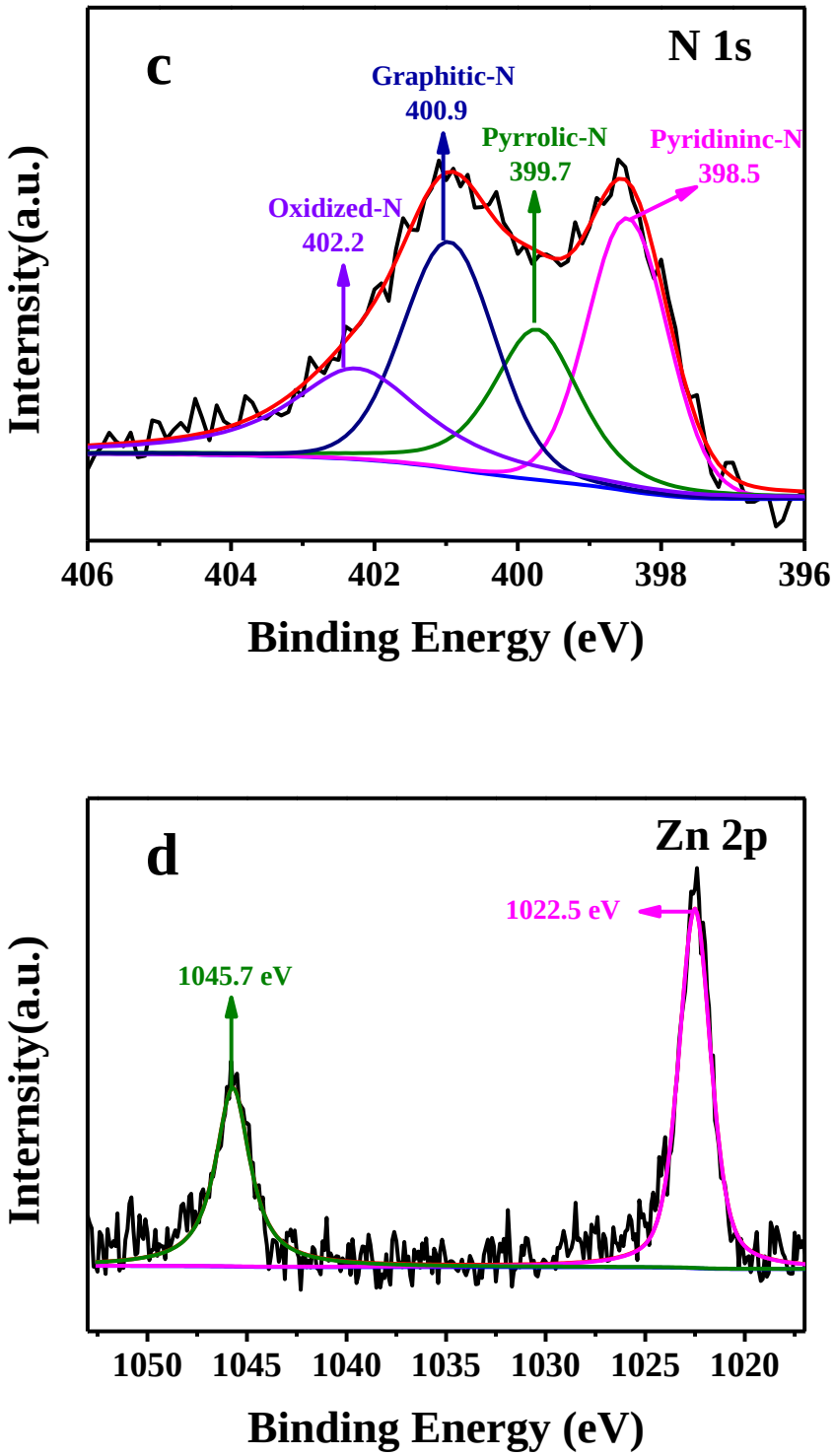

Figure 4. XPS survey spectrum of JZn-850: (a) XPS survey spectrum; (b) C1s, (c) N1s, and (d) Zn2p high-resolution spectrum.

This structure facilitates contact with the electrolyte, and accelerating the charge transfer rate [49]. In connection with the SEM image (Fig. 1c) and pore size analysis (Fig. 3b) above, we suggest that there are a number of irregular micropores, mesopores and macropores in the material.

Fig. 4 shows the XPS survey spectrum of JZn-850. The survey spectrum (Fig. 4a.) indicates that the C, N, O and Zn were present. Their contents were 90.96 at%, 3.40 at%, 5.18 at% and 0.46 at%, respectively. This suggests that Zn has not been completely removed. However, we did not find the presence of Zn in the XRD, for the content of zinc is too low, which is lower than the detection limit of the XRD instrument.

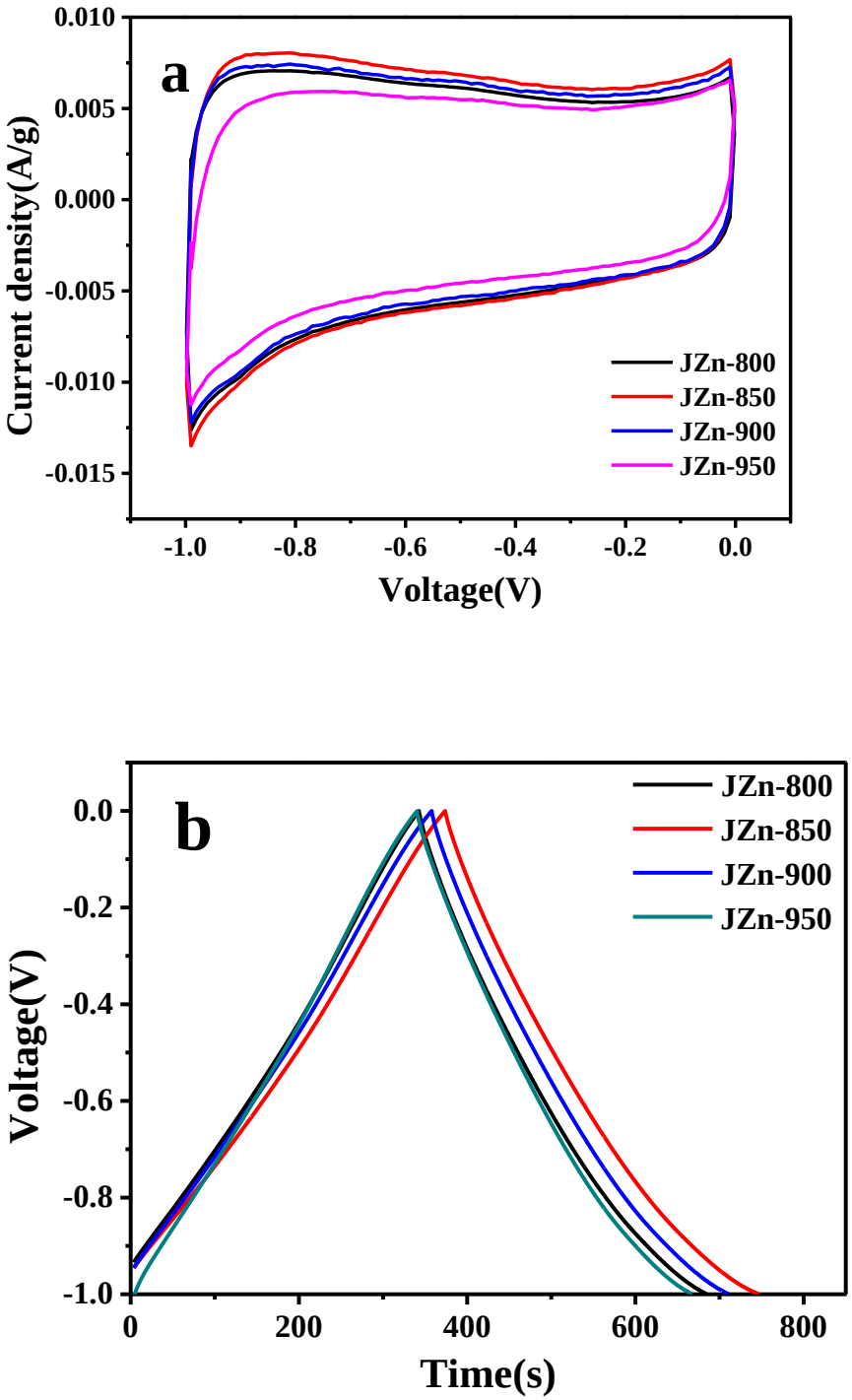

Figure 5. (a) CV curves of JZn-800, JZn-850, JZn-900, JZn-950 at the scanning rate of 5 mV s^{-1}. (b) GCD curves tested at a current density of 0.5 A g^{-1}.

The XPS high-resolution spectrum of C1s (Fig. 4b) can be deconvolved into four peaks at 284.8 eV, 285.7 eV, 286.5 eV and 289.2 eV. We can assign them to C-C bond, C-(O,N) bond, C-N bond, and N-C=O bond [50, 51]. That's because O and N are more electronegative than C. Their doping will change the charge distribution on adjacent C and lead to increased binding energy of C. Fig. 4c shows N1s can be divided into pyridinc-N (398.5eV), pyrrolic-N (399.7eV), graphitic-N (400.9eV) and oxidized-N (402.2eV) four different peaks [13, 52, 53]. Their contents were 28.7%, 20.8%, 28.2% and 22.3%, respectively.

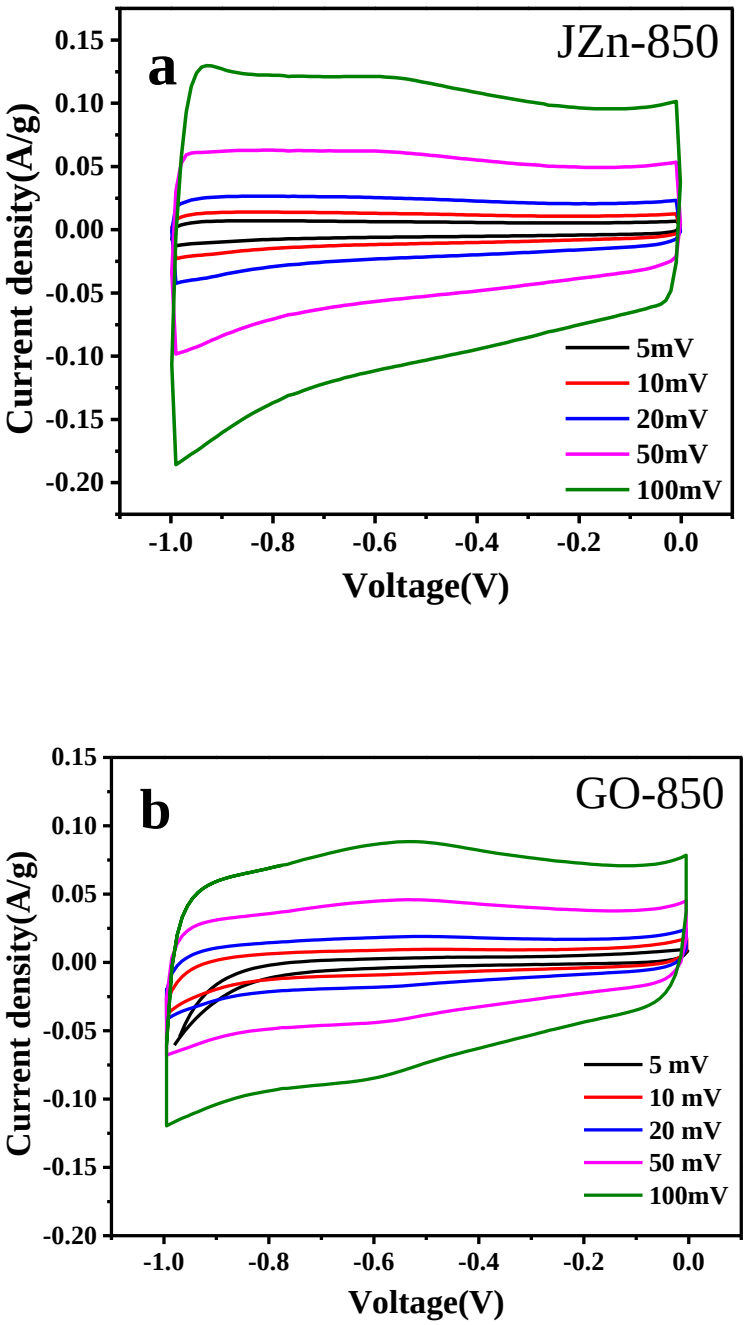

Figure 6. (a) CV curves of JZn-850 at different scan rates. (b) CV curves of GO-850 at different scan rates.

Some studies have shown that pyridinc-N, pyrrolic-N, and graphitic-N will tune the lewis basicity of next carbon atoms which can accelerate the transfer of electrons [43, 53, 54]. The total of pyridinc-N, pyrrolic-N, and graphitic-N in JZn-850 is 77.7%, which will be conducive to the charging and discharging of supercapacitors. Fig. 4d shows the XPS high-resolution spectrum of Zn2p, peaks at 1022.5eV and 1045.7eV can be classified as Zn2p 3/2(ground state) and Zn2 p1/2(excited state) of Zn(II) [55, 56]. This suggests that zinc is present mainly as an oxide in the sample JZn-850.

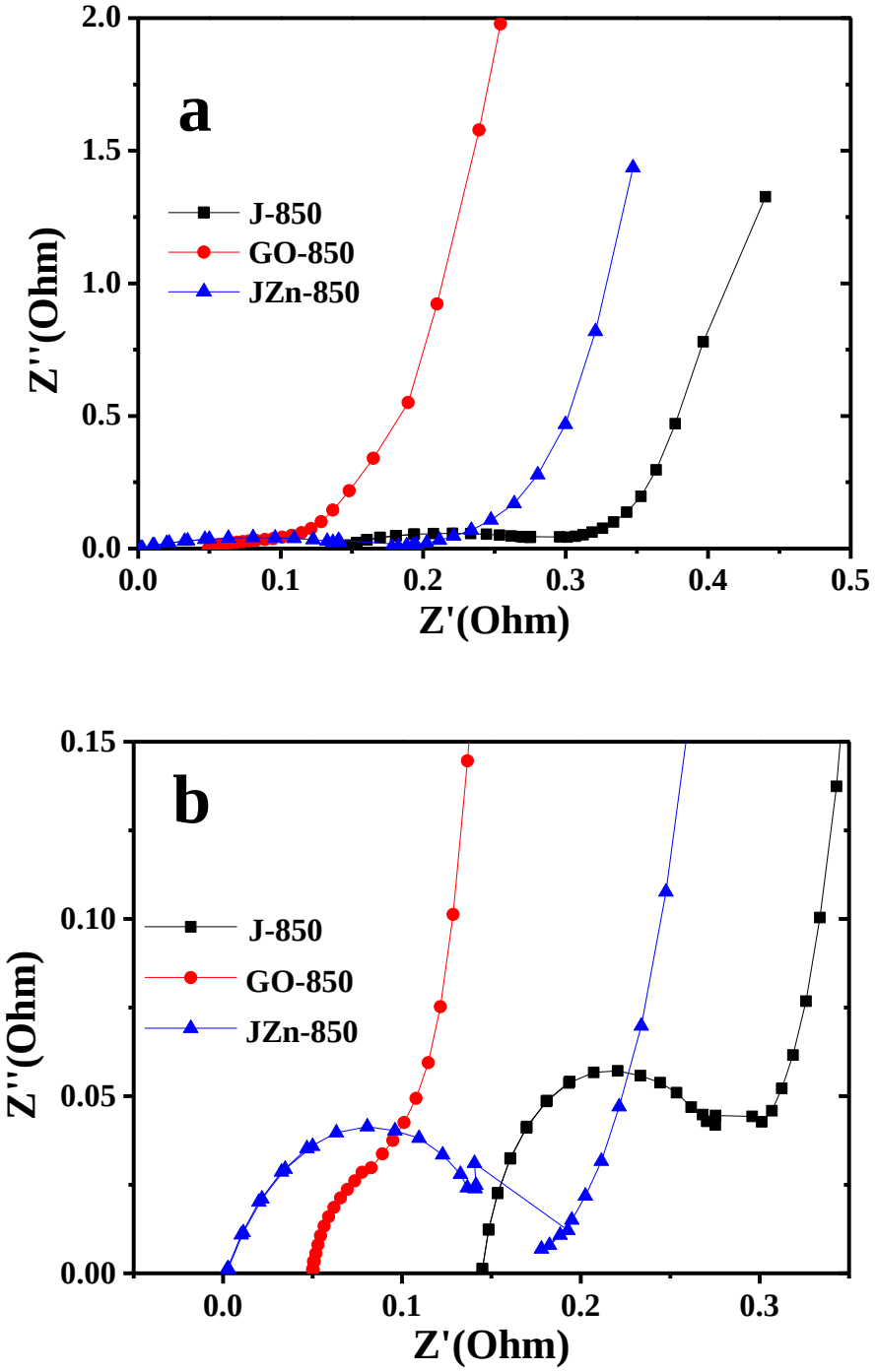

Figure 7. (a,b) The EIS spectrum of J-850, GO-850,and JZn-850.

Fig. 5a. shows CV curves of JZn-800, JZn-850, JZn-900, JZn-950 at the scanning rate of 5 mV s^{-1}. We can obserbe in the figure, JZn-850 has the largest area and the largest specific capacitance in the four samples. As Fig. 5b. shown, the specific capacitors of JZn-800, JZn-850, JZn-900 and JZn-950 are 170, 185, 176.2 and 164 F g^{-1}, respectively, at 0.5 A g^{-1}. We suggest that the optimum temperature for waste wine industry carbonization is 850 ^{o}C.

Fig. 6a shows CV curves of JZn-850 at different scan rates. After replacing the scanning rate, the CV curve remains in its original shape. Description JZn-850 has good stability. However, as Fig. 6b shown, with the change of scanning rate, the deformation of the CV curve of GO-850 is very obvious. This suggests that the JZn-850 has a more excellent stability than that of GO-850. Fig. 7a shows the EIS spectrum of frequency rate section. From the figure we can see that they have a large slope at low frequency range, indicating that they are conducive to internal ion transfer and diffusion, which indicate that all of these materials are conducive to rapid and high-power charge and discharge. In the high frequency band, the intercept and arc radius of JZn-850 is lower than J-850 and GO-850 **(Fig. 7a)**. This means that the internal resistance and leakage current resistance (or charge transfer resistance) of JZn-850 is smaller than that of J-850 and GO-850. It is further shown that JZn-850 is a more ideal electrode material for supercapacitor than that of the J-850 and GO-850.

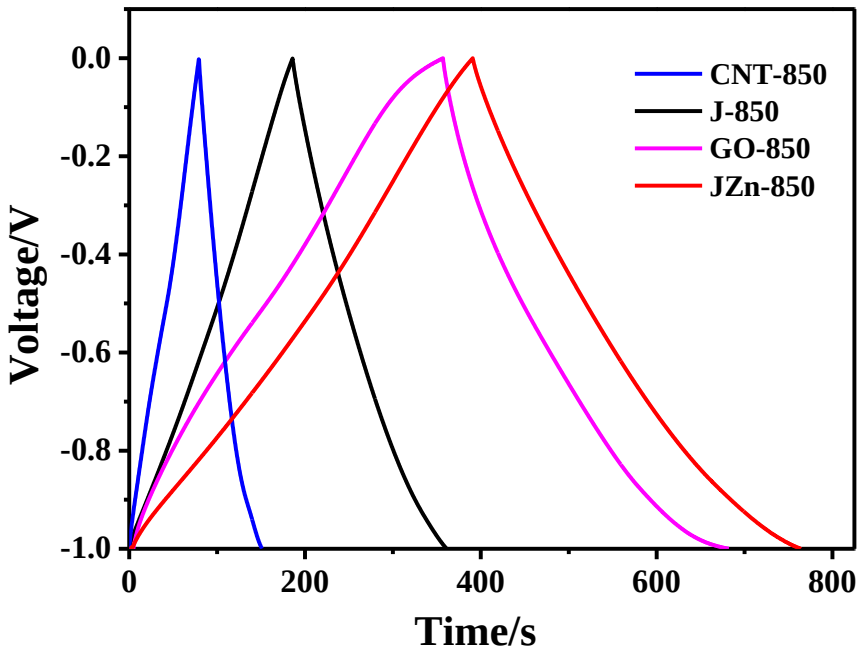

Figure 8. GCD curves tested of commercial carbon nanotubes (CNT-850), graphene oxide (GO-850), J-850 and JZn-850. (current density: 0.5 A g^{-1}) .

Fig. 8. shows the GCD curve of CNT-850, J-850, GO-850, JZn-850 at 0.5 A g^{-1}. The specific capacitors of CNT-850, J-850, GO-850, and JZn-850 are 37, 85, 162 and 185 F g^{-1}, respectively. JZn-850 has the higher specific capacitance than that of the CNT and GO, which suggest that JZn-850 has advantages over CNT and GO in supercapacitors as an electrode material. JZn-850 has the higher

specific capacitance than that of the J-850, shows that the energy storage performance of electrode carbon materials can be improved when preparing carbon materials after biomass activation. As listed in Table 1, the specific capacitance of JZn-850 is comparable with some other carbon materials, which demonstrates the superiority of JZn-850.

Table 1. Comparison of specific capacitance of JZn-850 with some other carbon materials

Materials	Current density(A g-1)	Electrolyte	specific capacitance(F g-1)	Reference
H_3PO_4/PANI/-800	0.05	6M KOH	154.4	[57]
PPZn	0.3	6M KOH	119.03	[58]
O-NQ/N-O-CNT	1	6M KOH	143.68	[59]
T/C1200	1	6M KOH	167	[60]
ACF	1	6M KOH	204.17	[61]
PCNS	0.2	6M KOH	169	[62]
SBA-15-MM	0.5	6M KOH	212.8	[63]
GO	0.5	6M KOH	154	[64]
rGO	0.5	6M KOH	120	[64]
CNT-850	0.5	6M KOH	37	This work
J-850	0.5	6M KOH	85	This work
GO-850	0.5	6M KOH	162	This work
JZn-850	0.5	6M KOH	187	This work

4. CONCLUSION

In this work, we successfully prepared a kind of activated carbon material with high BET specific surface area (1103 m^2 g^{-1}) from wine mash and zinc chloride. The specific capacitance of the material is 186 F g^{-1} and has good stability. In addition, the preparation process of the material is simple, the raw materials are rich, and the material is very environment-friendly and is suitable for industrial application. This also provides a reliable idea for the research of supercapacitors and lithium-ion batteries.

ACKNOWLEDGEMENTS
We gratefully acknowledge the financially supported by the National Science Foundation of China (51761006, 51671062), the National Key Research and Development Program of China (2018YFB1502103) and the National Science Foundation of Guangxi Province (2018JJA160046, AD17195073, 2017AD23029).

References

1. M.K. Debe, *Nature*, 486 (2012) 43-51.
2. S. Chen, S. Liu, A. Wen, J. Zhang, H. Nie, J. Chen, R. Zeng, Y. Long, Y. Jin, R. Mai, *Electrochim. Acta*, 271 (2018) 312-318.

3. Y. Zheng, L. Zhang, P. He, D. Dang, Q. Zeng, J. Zeng, M. Liu, *Electrocatalysis*, 9 (2018) 495-504.
4. H. Song, A. Tang, G. Xu, L. Liu, M. Yin, Y. Pan, *Int. J. Electrochem. Sc.*, 13 (2018) 4720-4730.
5. K. Deng, C. Li, X. Qiu, J. Zhou, Z. Hou, *Electrochim. Acta*, 174 (2015) 1096-1103.
6. Q. Yi, Y. Zhang, X. Liu, Y. Yang, *Sci China Chem*, 57 (2014) 739-747.
7. L. Yu, Q. Yi, G. Li, Y. Chen, X. Yang, *J. Electrochem. Soc.*, 165 (2018) A2502-A2509.
8. L. Yu, Q. Yi, X. Yang, G. Li, *Chemistryselect*, 3 (2018) 12603-12612.
9. J. Ding, S. Ji, H. Wang, H. Gai, F. Liu, B.G. Pollet, R. Wang, *Chem. Commun.*, 55 (2019) 2924-2927.
10. F. Liu, X. Yang, D. Dang, X. Tian, *ChemElectroChem*, 6 (2019) 2208-2214.
11. Y. Liu, Q. Sui, Y. Zou, C. Xiang, F. Xu, J. Xie, L. Sun, *Int. J. Electrochem. Sc.*, (2019) 5096-5106.
12. Y. Deng, Y. Xie, K. Zou, X. Ji, *J. Mater. Chem. A*, 4 (2016) 1144-1173.
13. H. Peng, F. Liu, X. Liu, S. Liao, C. You, X. Tian, H. Nan, F. Luo, H. Song, Z. Fu, P. Huang, *Acs Cata.*, 4 (2014) 3797-3805.
14. Y. Zhang, X. Li, P. Dong, G. Wu, J. Xiao, X. Zeng, Y. Zhang, X. Sun, *Acs Applied Materials & Interfaces*, 10 (2018) 42796-42803.
15. S. Dutta, A. Bhaumik, K.C.W. Wu, *Energ. environ. Sci.*, 7 (2014) 3574-3592.
16. G.-r. Xu, Y. Wen, X.-p. Min, W.-h. Dong, A.-p. Tang, H.-s. Song, *Electrochim. Acta*, 186 (2015) 133-141.
17. H. Yan, T. Li, Y. Lu, J. Cheng, T. Peng, J. Xu, L. Yang, X. Hua, Y. Liu, Y. Luo, *Dalton. Trans.*, 45 (2016) 17980-17986.
18. Y. Zou, C. Cai, C. Xiang, P. Huang, H. Chu, Z. She, F. Xu, L. Sun, H.-B. Kraatz, *Electrochim. Acta*, 261 (2018) 537-547.
19. T. Cetinkaya, R.A.W. Dryfe, *J. Power Sources*, 408 (2018) 91-104.
20. G. Bahuguna, P. Ram, R.K. Sharma, R. Gupta, *Chemelectrochem*, 5 (2018) 2767-2773.
21. S.-H. Lee, S. Choi, *Mater. Lett.*, 207 (2017) 129-132.
22. M. Lazzari, F. Soavi, M. Mastragostino, *Fuel Cells*, 10 (2010) 840-847.
23. R. Drummond, D.A. Howey, S.R. Duncan, *J. Power Sources*, 277 (2015) 317-328.
24. E. Lim, C. Jo, J. Lee, *Nanoscale*, 8 (2016) 7827-7833.
25. M.W. Verbrugge, P. Liu, *J. Electrochem. Soc.*, 152 (2005) D79-D87.
26. A. Celzard, F. Collas, J.F. Mareche, G. Furdin, I. Rey, *J. Power Sources*, 108 (2002) 153-162.
27. Y. Zhu, S. Murali, M.D. Stoller, K.J. Ganesh, W. Cai, P.J. Ferreira, A. Pirkle, R.M. Wallace, K.A. Cychosz, M. Thommes, D. Su, E.A. Stach, R.S. Ruoff, *Science*, 332 (2011) 1537-1541.
28. Q. Yi, Q. Chen, *Electrochim. Acta*, 182 (2015) 96-103.
29. Q. Yi, H. Chu, M. Tang, Z. Yang, Q. Chen, X. Liu, *J. Electroanal. Chem.*, 739 (2015) 178-186.
30. K. Deng, C. Li, X. Qiu, J. Zhou, Z. Hou, *J. Electroanal. Chem.*, 755 (2015) 197-202.
31. G.Y. Xu, J.P. Han, B. Ding, P. Nie, J. Pan, H. Dou, H.S. Li, X.G. Zhang, *Green Chem.*, 17 (2015) 1668-1674.
32. S. Song, F. Ma, G. Wu, D. Ma, W. Geng, J. Wan, *J. Mater. Chem. A*, 3 (2015) 18154-18162.
33. L. Fangfang, P. Hongliang, Y. Chenghang, F. Zhiyong, H. Peiyan, S. Huiyu, L. Shijun, *Electrochim. Acta*, 138 (2014) 353-359.
34. H. Peng, P. Huang, P. Yi, F. Xu, L. Sun, *J. Mol. Struct.*, 1154 (2018) 590-595.
35. E. Redondo, J. Segalini, J. Carretero-Gonzalez, E. Goikolea, R. Mysyk, *Electrochim. Acta*, 293 (2019) 496-503.
36. M. Genovese, J. Jiang, K. Lian, N. Holm, *J. Mater. Chem. A*, 3 (2015) 2903-2913.
37. A.M. Abioye, F.N. Ani, *Renew. Sust. Energy Rev.*, 52 (2015) 1282-1293.
38. A. Tang, Q. Zhong, G. Xu, H. Song, *Rsc Adv.*, 6 (2016) 84439-84444.
39. H. Song, A. Tang, G. Xu, L. Liu, Y. Pan, M. Yin, *Int. J. Electrochem. Sc.*, 13 (2018) 6708-6716.
40. Q. Yi, H. Chu, M. Tang, Y. Zhang, X. Liu, Z. Zhou, H. Nie, *Fuel Cells*, 14 (2014) 827-833.
41. Z. Deng, Q. Yi, G. Li, Y. Chen, X. Yang, H. Nie, *Electrochim. Acta*, 279 (2018) 1-9.
42. M.F. Chen, S.X. Jiang, C. Huang, X.Y. Wang, S.Y. Cai, K.X. Xiang, Y.P. Zhang, J.X. Xue,

Chemsuschem, 10 (2017) 1803-1812.
43. H. Peng, Z. Mo, S. Liao, H. Liang, L. Yang, F. Luo, H. Song, Y. Zhong, B. Zhang, *Sci. Rep.*, 3 (2013) 1765.
44. Y. Zhang, X. Li, M. Zhang, S. Liao, P. Dong, J. Xiao, Y. Zhang, X. Zeng, *Ceram. Int.*, 43 (2017) 14082-14089.
45. B. Zheng, H. Wang, Z. Wang, N. Ozaki, C. Hang, X. Luo, L. Huang, W. Zeng, M. Yang, J. Duan, *Chem. Commun.*, 52 (2016) 12988-12991.
46. H. Peng, S. Hou, D. Dang, B. Zhang, F. Liu, R. Zheng, F. Luo, H. Song, P. Huang, S. Liao, *Appl. Catal. B: Environ.*, 158-159 (2014) 60-69.
47. X. Qiao, H. Peng, C. You, F. Liu, R. Zheng, D. Xu, X. Li, S. Liao, *J. Power Sources*, 288 (2015) 253-260.
48. B. Zheng, L. Huang, X. Cao, S. Shen, H. Cao, C. Hang, W. Zeng, Z. Wang, *Crystengcomm*, 20 (2018) 1874-1881.
49. Y.L. Wang, B.B. Chang, D.X. Guan, X.P. Dong, *J. Solid State Electrochem.*, 19 (2015) 1783-1791.
50. J.E. KlembergSapieha, D. Poitras, L. Martinu, N.L.S. Yamasaki, C.W. Lantman, *J. Vac. Sci. Technol. A.*, 15 (1997) 985-991.
51. K. Shimizu, C. Phanopoulos, R. Loenders, M.-L. Abel, J.F. Watts, *Surf. Interface Anal.*, 42 (2010) 1432-1444.
52. P.H. Matter, L. Zhang, U.S. Ozkan, *J. Catal.*, 239 (2006) 83-96.
53. D. Guo, R. Shibuya, C. Akiba, S. Saji, T. Kondo, J. Nakamura, *Science*, 351 (2016) 361-365.
54. C. Long, J.L. Zhuang, Y. Xiao, M.T. Zheng, H. Hu, H.W. Dong, B.F. Lei, H.R. Zhang, Y.L. Liu, *J. Power Sources*, 310 (2016) 145-153.
55. K.R. Murali, *J. Phys. Chem. Solids*, 68 (2007) 2293-2296.
56. K. Shimazu, M. Takechi, H. Fujii, M. Suzuki, H. Saiki, T. Yoshimura, K. Uosaki, *Thin Solid Films*, 273 (1996) 250-253.
57. C.L. Wang, L. Sun, Y. Zhou, P. Wan, X. Zhang, J.S. Qiu, *Carbon*, 59 (2013) 537-546.
58. C.K. Sim, S.R. Majid, N.Z. Mahmood, *J. Alloys Compd.*, 803 (2019) 424-433.
59. J.F. Miao, X.X. Dong, Y.L. Xu, Z.Z. Zhai, L.H. Zhang, B. Ren, Z.F. Liu, *Org. Electron.*, 73 (2019) 304-310.
60. X.Y. Song, X.L. Ma, Y. Li, L. Ding, R.Y. Jiang, *Appl. Surf. Sci.*, 487 (2019) 189-197.
61. P. Chang, Z.H. Qin, *Int. J. Electrochem. Sc.*, 12 (2017) 1846-1862.
62. Y. Wen, K. Kierzek, J. Min, X. Chen, J. Gong, R. Niu, X. Wen, J. Azadmanjiri, E. Mijowska, T. Tang, *J. Appl. Polym. Sci.*, 0 48338.
63. K. Wu, Q.M. Liu, *Appl. Surf. Sci.*, 379 (2016) 132-139.
64. L.W. Le Fevre, J.Y. Cao, I.A. Kinloch, A.J. Forsyth, R.A.W. Dryfe, *Chemistryopen*, 8 (2019) 418-428.